Intriguing viscosity effects in confined suspensions: A numerical study

Y. Davit and P. Peyla[a]

Laboratoire de Spectrométrie Physique, Université Joseph Fourier - Grenoble 1, BP87, F-38402 Saint Martin d'Hères, France, EU

PACS 47.57.E- – Suspensions
PACS 47.57.Qk – Rheological aspects
PACS 47.11.-j – Computational methods in fluid dynamics

Abstract – The effective viscosity of dilute and semi-dilute suspensions in a shear flow in a microfluidic configuration is studied numerically. The suspension is composed of monodisperse and non-Brownian hard spherical buoyant particles confined between two walls in a shear flow. An abrupt change of the viscosity behaviour occurs with strong confinements: when the wall-to-wall distance is below five times the radius of the particles, we obtain a change of the sign of the contribution of the hydrodynamic interactions to the effective viscosity. This effect is the macroscopic counterpart of the peculiar micro-hydrodynamics of confined suspensions due to the influence of walls. In addition, for higher concentrations (above 25%), we find that the viscosity meets a minimum when the inter-wall distance is around five times the sphere radius. This phenomenon is reminiscent of the Fahraeus-Lindqvist effect for blood confined in small capillaries. However, we show that for sheared confined semi-dilute suspensions, the physical origin of this minimum is not due to a migration effect but to the change of hydrodynamic interactions.

Introduction. – Solid particles suspended in a conventional liquid form a suspension. This composite fluid constitutes a widespread fluid material in nature as well as in industry [1]. The particles can be spatially confined in porous media, in biological capillaries or in microfluidic devices [2]. In these situations, rheological phenomena due to interactions between device boundaries and fluid constituents become much more important than in conventional cases. These interactions of hydrodynamic origin play a crucial role, particularly, they appear to affect notably the effective viscosity $\langle\eta\rangle_{eff}$ of confined sheared suspensions as shown in this letter. Of course, considering microfluidics devices, pressure-driven flows are very important. However, in order to understand the role of the walls on hydrodynamic interactions, it is preferable to study a suspension in a simple shear geometry in order to estimate its effective viscosity. In addition, it should allow rheologists to easily compare their experimental results with our numerical predictions.

It is well known that the relative viscosity of a semi-dilute sheared suspension follows a virial expansion:

$$\frac{\Delta\eta}{\eta_0} = \frac{\langle\eta\rangle_{eff} - \eta_0}{\eta_0} = [\eta]_1\phi + [\eta]_2\phi^2 + \mathcal{O}(\phi^3), \qquad (1)$$

where ϕ is the volume fraction defined as the volume of the particles normalized to the total volume of the suspension and η_0 is the viscosity of the fluid. For a non-confined suspension of hard spheres, the linear term (the intrinsic viscosity) is $[\eta]_{1,\infty} = 2.5$ as calculated by Einstein [3] for a strong dilution (*i.e.* particles are far enough not to interact with each other through hydrodynamics). Subscript ∞ indicates that we refer to non-confined suspensions. When increasing ϕ, the semi-dilute regime is reached, the particles get closer than in the dilute regime and start to interact hydrodynamically. Batchelor and Green [4] showed that the hydrodynamic interactions contribute to the second order in ϕ. They found $[\eta]_{2,\infty} = 5.2 \pm 0.3$ for a non-confined and non-Brownian suspension where the particles are uniformly distributed. Since then, a more precise estimation of $[\eta]_{2,\infty} = 5.0$ has been achieved by Cichoki and Felderhof [5].

We find that when the wall-to-wall distance (or gap) w decreases, the linear term $[\eta]_1$ (dominant for strongly dilute cases, *i.e.* $\phi \ll 1$) increases. This is due to dissipation which is enhanced for smaller gaps. However,

[a] E-mail: philippe.peyla@ujf-grenoble.fr

the quadratic term $[\eta]_2$ decreases to zero when $w \approx 5R$ and becomes negative for smaller gaps ($2R < w < 5R$), R being the sphere radius. This intriguing behaviour is due to the specific hydrodynamic interactions of strongly confined suspensions. We also find that the effective viscosity exhibits a minimum as a function of the gap for concentrations $\phi > 25\%$. We show that this minimum is a consequence of the change of the hydrodynamic interactions when the suspension is getting confined and not of particles structuring or demixing as, for example, it is the case for blood confined in small capillaries (Fahraeus-Lindqvist effect) [6].

Model and numerical method. – The suspended elements are monodisperse spheres of radius R that are free to rotate. In the present work, the Brownian motion is not included since we consider rather large objects like cells, vesicles or capsules. Note that we consider rigid particles both for simplicity and in order not to include further ingredients like deformability. The spheres are suspended in a Newtonian fluid of viscosity η_0 confined between two plates. The two plates located at $x = \pm w/2$ move at $v_z = \pm v_0$, respectively, so that the shear rate is $\dot{\gamma} = 2v_0/w$. No-slip conditions are used at the fluid/plates interface. The confinement is measured by the dimensionless gap $c = w/2R$. As an initial condition, we randomly and homogeneously distribute the spheres (taking care to avoid any overlaps). The fluid equation of motion around the spheres takes the usual form

$$\rho(\partial_t + \mathbf{v} \cdot \nabla)\mathbf{v} = \nabla \cdot \sigma, \tag{2}$$

with the incompressibility condition $\nabla \cdot \mathbf{v} = 0$, where $\mathbf{v}$ is the velocity field and ρ is the fluid density. Note that we deal with buoyant particles with the same density ρ. The stress tensor reads

$$\sigma_{ij} = -P\delta_{ij} + \eta_0[\partial_i v_j + \partial_j v_i], \tag{3}$$

where P is the pressure field and η_0 is the viscosity of the solvent. Usually, the spheres are taken into account through moving boundary conditions which are quite difficult to handle. This problem will be circumvented as follows. We use the "fluid particle dynamics" (FPD) originally developed by Tanaka and Araki [7] and extended to $3D$ by one of the authors [8]. Note that other methods such as lattice Boltzmann methods [9,10] or Stokesian dynamics [11,12] could be used as well. The advantage of the FPD is to explicitly avoid tracking the particles and thus to avoid applying boundary conditions on a moving boundary. In this method, the particles are defined as high-viscosity regions in comparison to that of the solvent. Therefore, the flow field is defined in the entire domain (and not only outside the spheres) bounded by the walls. Thus, at each time step eq. (2) is solved outside and inside the particles except that the viscosity η_0 is replaced by a viscosity field. We briefly summarize the main points of the numerical method, details can be found in the original Tanaka's and Araki's paper [7].

The presence of the particle number n is accounted for via an auxiliary field,

$$\varphi_n(\mathbf{r}) = \{1 + \tanh[(a - |\mathbf{r} - \mathbf{r}_n|)/\zeta]\}/2, \tag{4}$$

where ζ represents the fluid-particle interface thickness and $\mathbf{r}_n$ is the off-lattice center of the particle n. Thus, the radius of a sphere is $R = a + \zeta$. We choose $a = 2\delta$ and $\zeta = \delta$ where δ is the mesh size. In other words, the difficulty of the sharp interface between each sphere and the fluid is circumvented by introducing a diffuse (albeit abrupt enough) interface. The idea then is to introduce a viscosity field such as

$$\eta(\mathbf{r}) = \eta_0 + (\eta_p - \eta_0)\sum_{n=1}^{N} \varphi_n, \tag{5}$$

where N is the total number of spheres. This ensures that far enough from the particle, the local viscosity is $\eta = \eta_0$ (the solvent viscosity) and inside the particle we have $\eta = \eta_p$ (the particle viscosity). The viscosity contrast is fixed to $\eta_p/\eta_0 = 100$. This choice is made to avoid any recirculation of the fluid inside the spheres, which can thus be considered as rigid [7]. Equation (2) is solved on a Mac grid [13] where pressure P, viscosity η (instead of η_0), and stress are calculated at the center of each cubic mesh i of size $\delta \times \delta \times \delta$ located in (X_i, Y_i, Z_i), while fluid velocity components are calculated at the center of each face of the mesh. This ensures that each term involved in eq. (2) when it is discretized is calculated at the same point of the mesh grid [13]. In order to get the right value of the volume fraction ϕ, the volume of the particles must be calculated carefully by taking into account the diffuse interface (of size ζ) of each particle. Due to the discretization of the solvent, we compute the volume fraction by counting the number N_c of cells of viscosity at least 10% bigger than the solvent one $\eta_0 = 1$. For each particle with size parameters such as $a = 2\delta$ and $\zeta = \delta$, we get $119 < N_c/N < 125$. This number slightly fluctuates since particles are off-lattice while the viscosity field is averaged in each cell. The volume fraction is calculated as $\phi = N_c/N_{box}$, where N_{box} is the total number of cells in the simulation box. It gives an effective radius $R_{eff} = (3N_c/4\pi N)^{1/3}\delta$ such that $3.05\delta < R_{eff} < 3.1\delta$, which is close to the value of $R = a + \zeta = 3\delta$.

The numerical procedure is as follows: for each time step $\delta t = 0.001$, pressure and velocity are calculated following a standard projection method ensuring the incompressibility of the fluid [13]. A constant value for $\dot{\gamma} = 10^{-5}/\delta t = 10^{-2}$ is used for the different studied values of the gap. Inertia is negligible in eq. (2) since only small Reynolds numbers are considered here. The typical simulation box sizes are $L_Y = 79\delta$, $L_Z = 60\delta$, while $L_X = w$ varies from 10δ to 79δ. Here, $\delta = 1$. The boundary conditions are such that the fluid velocity is imposed on X, Y box boundaries ($v_Z(X, Y = \pm L_Y/2, Z) = \dot{\gamma}X$ and $v_Z(X = \pm w/2, Y, Z) = \pm v_0$), while periodic boundary conditions are adopted in the Z-direction. For each time

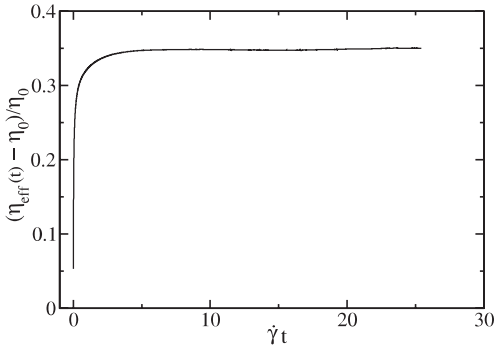

Fig. 1: Averaged relative viscosity as a function of rescaled time $\dot{\gamma}t$ with $\dot{\gamma} = 10^{-2}$. For a gap $c = 13.2$ and a volume fraction $\phi = 11\%$, after an initial transient regime, the viscosity reaches a plateau.

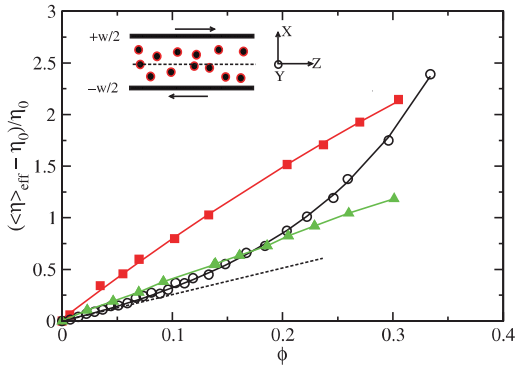

Fig. 2: Relative viscosity as a function of ϕ for different gaps (circles $c = 13.2$; triangles-up $c = 2.5$; squares $c = 1.67$). The solid curves are just guide for the eyes. The dashed lines indicate slopes at the origin for the two extreme values of c. The drawing gives a schematic view of the studied system.

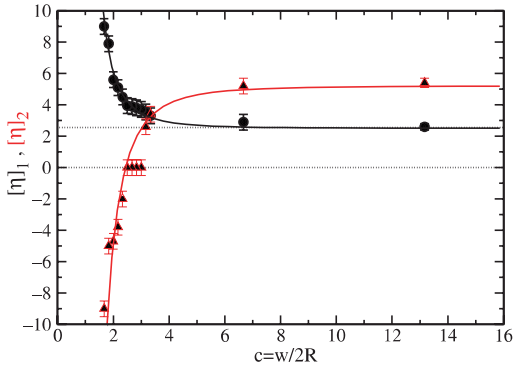

Fig. 3: Coefficients $[\eta]_1$ (circles) and $[\eta]_2$ (triangles) as a function of the normalized gap c. The curves are just guides for the eyes. Error bars are due to the fit uncertainty.

step, the off-lattice center $\mathbf{r}_n$ of the particle n is moved as follows: $\mathbf{r}_n(t+\delta t) = \mathbf{r}_n(t) + \delta t\, \bar{\mathbf{v}}_n(t)$, where $\bar{\mathbf{v}}_n(t)$ is the fluid velocity averaged on the high-viscosity region surrounding the center of the sphere n at time t. It ensures the shape preserving of the particles. The viscosity field is then reconstructed [7] considering the new positions of the spheres at time $t+\delta t$. This gives rise to a new bulk viscosity field. This field is injected into eq. (2) which is solved again for $t+\delta t$. In previous papers [7,8], tests on this method have been performed to prove its reliability.

Results. – The effective viscosity of the suspension is evaluated by calculating the tangential force per unit surface exerted by the plates on the fluid: $f_z^{\pm}(t) = \bar{\sigma}_{xz}(x = \pm w/2,\, t)\, n_x$ which is necessary to maintain a constant velocity $\pm v_0$ on the upper $(+)$ and lower $(-)$ plates. The unit vector $\mathbf{n}$ is normal to the fluid/plate interface. $\bar{\sigma}_{xz}$ represents the average of $\sigma_{xz}(\pm w/2)$ on the whole surface of the fluid in contact with the plates. The time-dependent effective viscosity is thus $\eta_{eff}(t) = 1/2\,[f_z^+(t) - f_z^-(t)]/\dot{\gamma}$.

Initially, we start with a random distribution of spheres. After a transient regime, the effective viscosity reaches a plateau and remains stable for thousands of time steps (fig. 1). By eliminating the initial transient regime and averaging the plateau values, we finally obtain the averaged effective viscosity $\langle\eta\rangle_{eff}$ calculated for a given confinement and a given initial configuration (fig. 1).

In fig. 2, we show the relative effective viscosity $\Delta\eta/\eta_0$ obtained numerically as a function of the volume fraction ϕ for three different confinements. When decreasing the gap w at constant R, we can explicitly see that the curvature of the curves decreases and becomes negative, while the linear term increases when the dimensionless gap c decreases.

We fit $\Delta\eta/\eta_0(\phi)$ for each gap value. We performed the fit below $\phi < 15\%$ with a 2nd-degree polynomial expression in ϕ as in eq. (1). As a matter of fact for $\phi < 15\%$ the contribution of higher-order terms is found to be negligible. Thus, we obtain the values of the coefficients $[\eta]_1$ and $[\eta]_2$ as functions of the dimensionless gap c (fig. 3).

A rapid variation of these two coefficients is observed when the inter-wall distance w becomes smaller than $5R$.

For a non-confined suspension (subscript ∞), we obtain the values $[\eta]_{1,\infty} = 2.6 \pm 0.2$ and $[\eta]_{2,\infty} = 5.4 \pm 0.5|$. Here, non-confined means that we perform our calculations with large values of the gap. The largest value that we use is $c = 13.2$ for which the parameters $[\eta]_1$ and $[\eta]_2$ reach their non-confined values within the error bars. Therefore, we assume that the confinement $c = 13.2$ can be considered as close enough to a non-confined case. Einstein's [3] theoretical value of $[\eta]_{1,\infty} = 2.5$ is quite well recovered. It means that our estimation of the volume fraction is precise enough. The theoretical value $[\eta]_{2,\infty} = 5.0$ [5] is also recovered within the error bars ± 0.5. This uncertainty is due to the quadratic polynomial fit done on a finite set of points with error bars. The main source of uncertainty of the numerical method is due to the slight dependence of the effective viscosity on local non-uniformity of the initial distribution of particles. In dilute and semi-dilute regimes, this kind of non-uniformity remains during the shear. This problem is usually cured by using more particles within a bigger simulation box (at constant ϕ) or by averaging

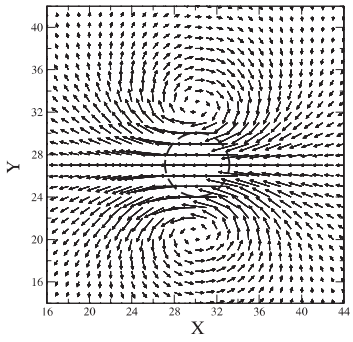

Fig. 4: Numerical velocity field $\delta\mathbf{v}$ in the equatorial plane (YOZ) of a sphere confined in a shear (the particle region is indicated with a dashed circle). The velocity field is such that $\delta\mathbf{v} = \mathbf{v} - \mathbf{v}_{shear}$, where $\mathbf{v}_{shear} = (0, 0, \dot{\gamma}X)$ is the velocity field in the absence of particles. The field $\delta\mathbf{v}$ is the additional flow created by an off-centered spherical particle which is confined along the Z-axis with $c = 1.67$. The particle clearly creates a conterflow for other particles located along the Y-axis. $\delta\mathbf{v}$ is similar to the velocity field considered in ref. [15].

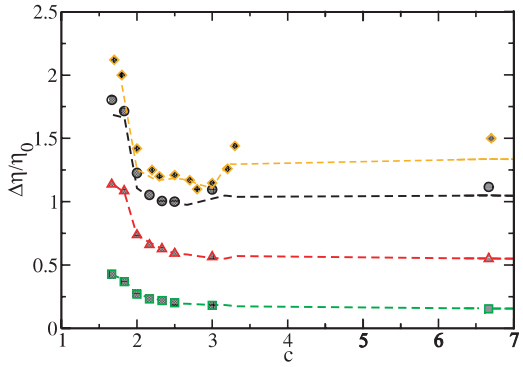

Fig. 5: Relative viscosity as a function of the dimensionless gap c for different values of ϕ: $\phi = 30\%$ (diamonds), $\phi = 25\%$ (circles), $\phi = 15\%$ (triangles), $\phi = 5\%$ (squares). The dashed curves are obtained using eq. (1) and the values of coefficients $[\eta]_1$ and $[\eta]_2$ as functions of c (fig. 3).

the effective viscosity on several runs using different initial configurations. Of course, these two procedures are computer-time consuming, especially in $3D$, but they are feasible with the help of a parallel version of the program which is under elaboration. We also perform a fit of the relative viscosity by the Krieger and Dougherty empirical formula [14]: $\Delta\eta/\eta_0 = (1 - \phi/\phi_m)^{-\alpha\phi_m} - 1$ gives $\phi_m \approx 0.635$ and $\alpha \approx 2.56$ in good agreement with the values $[\eta]_{1,\infty} = \alpha$ and $[\eta]_{2,\infty} = 1/2\,\alpha(1 + \alpha\phi_m)/\phi$ given above.

When increasing the confinement (smaller values of c), $[\eta]_1$ increases since the dissipation increases when walls are getting closer. The $[\eta]_2$ values decrease and cancel out when the gap $w \approx 5R$. For stronger confinements ($2R < w < 5R$), $[\eta]_2$ becomes negative. This means that the contribution of the hydrodynamic interactions to the effective viscosity becomes negative. This reveals the peculiar hydrodynamic behaviour of confined suspensions due to the influence of walls.

Recently, it has been experimentally [15] and theoretically [16,17] shown that hydrodynamic interactions between particles behave abnormally when the suspension is confined between two planar walls in a Hele-Shaw configuration. When the gap is slightly larger than the spherical-particles diameter, one deals with a quasi-2D (Q2D) suspension. Cui *et al.* [15] experimentally showed that an anti-drag effect holds between two particles moving perpendicularly to their connecting line. One should recover a signature of these remarkable Q2D microscopic hydrodynamic properties in the rheology —a macroscopic property— of confined semi-dilute suspensions through the quadratic ϕ-dependence of the effective viscosity. For non-confined suspensions, the drag effect between interacting particles enhances the viscosity and $[\eta]_{2,\infty}$ has a positive value. An anti-drag effect can explain the change of the sign of this term for confined suspensions. Therefore, the fact that the contribution of hydrodynamic interactions to the viscosity becomes negative could be traced back to this peculiar interaction effect. We have calculated the velocity field created by a single force-free sphere between two close walls ($c = 1.67$). The induced flow thus created can push back another sphere aligned along the Y-axis. This flow is at the origin of the anti-drag effect measured by Cui *et al.* [15]. In fig. 4, we show the velocity field $\delta\mathbf{v} = \mathbf{v} - \mathbf{v}_{shear}$, where $\mathbf{v}_{shear} = (0, 0, \dot{\gamma}X)$ is the velocity field in the absence of particles (see fig. 4). We obtain the same velocity field as the one that is created by a point-force in the middle of two walls and parallel to the walls [15]. It is also equivalent to a force dipole in the absence of walls.

At present, further studies are needed before obtaining a clear answer. To our knowledge, a full non-perturbative theory dealing with the influence of walls on coefficient $[\eta]_1$ and $[\eta]_2$ is still lacking [18].

Note that around $c \approx 1$ a solid friction should occur between particles and walls. In order to avoid this effect, which is not taken into account in our model, we limit ourselves to the values $c > 1.67$.

We find another interesting effect which is a direct consequence of the peculiar behaviour of hydrodynamic interactions in confined suspensions. At higher concentrations ($\phi > 25\%$), we find that the viscosity meets a minimum when the inter-wall distance is such that $w \sim 5R$ (fig. 5). For smaller concentrations, this phenomenon is not observed. This looks very similar to the Fahraeus-Lindqvist effect which is very well known for blood flowing through capillaries of different diameters [6]. The apparent viscosity of blood meets a minimum when the diameter is comparable to the red blood cells size and when the concentration of cells is higher than 20%. The Fahraeus-Lindqvist effect is due to a migration of the cells to the center of the parabolic flow in the capillary where they form rouleaux [6,19]. As shown below, the minimum we obtained is not mainly due to a migration but to the

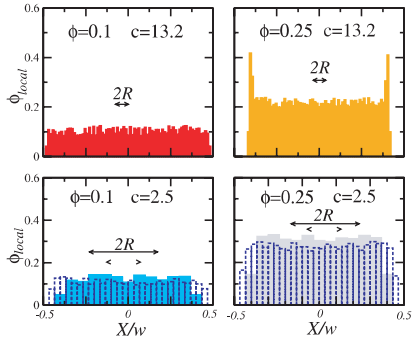

Fig. 6: Local volume fraction $\phi_{local}(X)$ as a function of X/w for two different values of ϕ and c. Each bar represents a layer located in X of one-mesh size and parallel to the plates. A depletion layer of about $2R$ is only observed for non-confined suspensions at $\phi = 25\%$. In the other cases, a lubrication fluid layer is observed. The double arrow represents the diameter of a particle. For the stronger confinement ($c = 2.5$) two different meshings have been used.

sign change of $[\eta]_2$ when the suspension is sufficiently confined.

In order to estimate the migration of spheres perpendicularly to the flow, we calculate a local volume fraction $\phi_{local}(X)$. It is the volume fraction averaged on all the cells located at height X between the plates ($-1/2 < X/w < 1/2$). As a matter of fact, a depletion near the walls is observed for high concentrations ($\phi \geqslant 25\%$) in non-confined situations. But, such a depletion is not observed for confined suspensions at any concentration: averaging on thousands of time steps, the distribution of spheres is rather uniform between the walls (see fig. 6). The absence of depletion at low concentration can be explained by the fact that for negligible Reynolds number, a single sphere is not submitted to a force normal to a close wall. Therefore, a depletion near the walls is due to a collective effect and is observed at relatively high concentration (here, for $\phi > 25\%$). Note that a lubrication fluid layer of one- or two-mesh size is always present between the walls and the particles. Note that migration perpendicular to the flow is a usual phenomenon also observed for solid particles in the case of pressure-driven flows [20]. In order to verify that migration perpendicularly to the flow has no effect on the minimum, we also performed simulations with a very small value $\dot{\gamma} = 10^{-7}/\delta t = 10^{-4}$. It allows us to calculate the averaged value of the effective viscosity on a time scale smaller than $\dot{\gamma}^{-1}$ (*i.e.* the spheres remain globally immobile during the simulation). The value of the viscosity so obtained are in good agreement with those obtained at stronger $\dot{\gamma}$ except for high concentrations and non-confined cases where the migration takes place and affects the viscosity.

So, unlike the Fahraeus-Lindqvist effect the minimum is not due to a migration of the particles perpendicularly to the flow. It is the result of the opposite variation of $[\eta]_1$ and $[\eta]_2$ as functions of c (fig. 3). As a matter of fact, we make the crude assumption that $\Delta\eta/\eta_0$ is still well described by the expansion (1) when ϕ is bigger than 15%. The plot of $[\eta]_1\phi + [\eta]_2\phi^2$ at constant ϕ as a function of c clearly shows a minimum around $w/R \approx 5$ for $\phi \geqslant 25\%$ (fig. 5). Of course, the agreement is good for small concentrations ($\phi < 15\%$) for which expression (1) is well verified. High-order terms in ϕ explain the difference between the curve and the calculated points for $\phi = 25\%$ or $\phi = 30\%$. But despite this difference, the presence of the minimum is clearly reproduced.

Conclusion. – Our main result is that the quadratic ϕ-dependence of the relative viscosity becomes negative for confined suspensions below $c = w/2R \approx 2.5$. Some preliminary experimental results [21] tend to confirm our numerical predictions. Another result is a consequence of the first one: the viscosity meets a minimum for the same c value. Several questions deserve future considerations. A full theory including walls to provide the confinement dependence of coefficients $[\eta]_1$ and $[\eta]_2$ is still lacking. Since a direct simulation is used, any type of geometry (such as pressure-driven flows, with branching, constrictions, ...) could be implemented as well. This should open interesting lines of inquiries towards the elaboration of prototypical devices for the sorting and guidance of suspended objects in microfluidics.

* * *

We thank C. Verdier and C. Misbah for their very constructive comments.

REFERENCES

[1] Russel W. B., Saville D. A. and Schowalter W. R., *Colloidal Dispersions* (Cambridge University Press, New York) 1989.
[2] Whitesides G. M. and Stroock A. D., *Phys. Today*, **54**, issue No. 6 (2001) 42.
[3] Einstein A., *Ann. Phys. (Leipzig)*, **19** (1906) 289; **34** (1911) 591.
[4] Batchelor G. K. and Green J. T., *J. Fluid. Mech.*, **56** (1972) 401.
[5] Cichoki B. and Felderhof B. U., *J. Chem. Phys.*, **89** (1988) 1049.
[6] Pries A. R., Neuhaus D. and Gaehtgens P., *Am. J. Physiol. Heart Circ. Physiol.*, **263** (1992) 1770.
[7] Tanaka H. and Araki T., *Phys. Rev. Lett.*, **85** (2000) 1338.
[8] Peyla P., *Eur. Phys. Lett.*, **80** (2007) 34001.
[9] Kromkamp J., van den Ende D., Kandhai D., van der Sman R. and Boom R., *Chem. Eng. Sci.*, **61** (2006) 858.
[10] Heemels M. W., Hagen M. H. J. and Lowe C. P., *J. Comput. Phys.*, **164** (2000) 48.
[11] Philips R. J. and Brady J. F., *Phys. Fluids*, **31** (1988) 3462.
[12] Pesché R. and Nägele G., *Europhys. Lett.*, **51** (2000) 584.

[13] Peyret R. and Taylor T. D., *Computational Methods for Fluid Flow* (Springer-Verlag, New York) 1963, p. 160.
[14] Krieger I. M. and Dougherty T. J., *Trans. Soc. Rheol.*, **3** (1959) 137.
[15] Bianxiao Cui, Diamant H., Binhua Lin and Rice S. A., *Phys. Rev. Lett.*, **92** (2004) 258301.
[16] Alvarez A. and Soto R., *Phys. Fluids*, **17** (2005) 93103.
[17] Bhattacharya S., Blawzdziewicz J. and Wajnryb E., *J. Fluid. Mech.*, **541** (2005) 263.
[18] Note that a perturbative theory has been done for $c \gg 1$ and $\phi \ll 1$: Guth E. and Simha R., *Kolloid*, **266** (1936); Happel J. and Brenner H., *Low Reynolds Number Hydrodynamics* (Martinus Nijhoff Publishers, The Hague) 1983, p. 444.
[19] Yaling Liu and Wing Kam Liu, *J. Comput. Phys.*, **220** (2006) 139.
[20] Frank S., Anderson D., Weeks E. R. and Morris J. F., *J. Fluid Mech.*, **493** (2003) 363.
[21] Verdier C., in preparation.